

## A POSSIBLE MAGNETAR NATURE FOR IGR J16358–4726

S. K. PATEL,<sup>1,2</sup> J. ZURITA,<sup>3</sup> M. DEL SANTO,<sup>4</sup> M. FINGER,<sup>2</sup> C. KOUVELIOTOU,<sup>1</sup> D. EICHLER,<sup>5</sup> E. GÖĞÜŞ,<sup>6</sup>  
P. UBERTINI,<sup>4</sup> R. WALTER,<sup>3</sup> P. WOODS,<sup>2</sup> C. A. WILSON,<sup>4</sup> S. WACHTER,<sup>7</sup> AND A. BAZZANO<sup>4</sup>

Received 2006 May 25; accepted 2006 October 16

### ABSTRACT

We present detailed spectral and timing analysis of the hard X-ray transient IGR J16358–4726 using multisatellite archival observations. A study of the source flux time history over 6 yr suggests that lower luminosity transient outbursts can be occurring in intervals of at most 1 yr. Joint spectral fits of the higher luminosity outburst using simultaneous *Chandra* ACIS and *INTEGRAL* ISGRI data reveal a spectrum well described by an absorbed power-law model with a high-energy cutoff plus an Fe line. We detected the 1.6 hr pulsations initially reported using *Chandra* ACIS also in the *INTEGRAL* ISGRI light curve and in subsequent *XMM-Newton* observations. Using the *INTEGRAL* data, we identified a spin-up of 94 s ( $\dot{P} = 1.6 \times 10^{-4}$ ), which strongly points to a neutron star nature for IGR J16358–4726. Assuming that the spin-up is due to disk accretion, we estimate that the source magnetic field ranges between  $10^{13}$  and  $10^{15}$  G, depending on its distance, possibly supporting a magnetar nature for IGR J16358–4726.

*Subject headings:* pulsars: individual (IGR J16358–4726)

*Online material:* color figure

### 1. INTRODUCTION

IGR J16358–4726 belongs to a new class of transient hard X-ray sources discovered with ESA’s *International Gamma-Ray Astrophysics Laboratory* (*INTEGRAL*; Winkler et al. 2003). Kuulkers (2005) describes the spectral and temporal properties of 10 of these sources discovered during regular scans of the Galactic plane with the Imager on board *INTEGRAL* (IBIS; Ubertini et al. 2003) through the end of 2004. They all exhibit very high intrinsic photoabsorption ( $N_{\text{H}} \gtrsim 10^{23} \text{ cm}^{-2}$ ) resulting in hard spectra with power-law spectral indices  $0.5 < \Gamma < 2.1$ . Four of these new transients exhibit long-period coherent pulsations in their high-energy (X-ray and  $\gamma$ -ray) fluxes in the range from 228 to  $\sim 5900$  s; so far they have been interpreted in the literature as high-mass X-ray binaries (HMXBs), based on their *spectral* similarities to other X-ray pulsars in these systems (Kuulkers 2005; Lutovinov et al. 2005). In only one of these sources, however, an orbital period of  $8.9 \pm 0.1$  days has also been found, supporting an HMXB nature for the source (IGR J16320–4751; Corbet et al. 2005).

Thus far, IGR J16358–4726 stands out as the sole outlier among these new *INTEGRAL* X-ray transients, having one of the hardest X-ray spectra and the longest period of all. The source was discovered with *INTEGRAL* by Revnivtsev et al. (2003) when it went into outburst on 2003 March 19. Our contemporaneous *Chandra* observations led to the discovery of large-amplitude coherent intensity modulations in the source light curve with  $P = 5880$  s (Kouveliotou et al. 2003a; Patel et al. 2004). Patel et al. (2004) showed that the source spectrum is extremely hard ( $\Gamma =$

0.5) and highly absorbed ( $N_{\text{H}} = 1.3 \times 10^{23} \text{ cm}^{-2}$ ), both during the outburst and in quiescence. Radio follow-up observations taken  $\sim 25$  and  $\sim 134$  days after the outburst resulted only in flux upper limits of 0.9 mJy (4.8 GHz; Patel et al. 2004) and 7.5 mJy (0.61 GHz; Pandey et al. 2006), respectively. S. Wachter et al. (2007, in preparation) report an accurate location of the source derived by off-axis point-spread function modeling of the initial *Chandra* observation. Their infrared observations, taken during the decaying tail of the source outburst, reveal a counterpart candidate for IGR J16358–4726 different than the one discussed by Kouveliotou et al. (2003b) and D’Amico et al. (2006); their data allow for both a low-mass X-ray binary (LMXB) and an HMXB system scenario (based only on the brightness of the counterpart). The candidate suggested by D’Amico et al. (2006) was observed during source quiescence; based on the lack of variability in the light curve of this putative counterpart, D’Amico et al. (2006) supported an HMXB nature of the source. Finally, based on the *INTEGRAL* survey observations, IGR J16358–4726 is thought to be located in the Norma arm of the Milky Way, at distance ranges of 5–6 kpc or 12–13 kpc, depending on which crossing of the arm with the line of sight is chosen (Lutovinov et al. 2005).

To date, there is no conclusive evidence for the nature of the IGR J16358–4726 period. Patel et al. (2004) suggested that the source is either a transient accreting pulsar with an unusually long spin period or a transient LMXB with a short orbit. Unraveling the nature of IGR J16358–4726 is essential, as this source provides an excellent avenue toward understanding the new class of *INTEGRAL* objects. Here we present a study of the source flux history and spectra using combined X-ray and  $\gamma$ -ray observations with *ASCA*, *BeppoSAX*, *INTEGRAL*, *Chandra*, and *XMM-Newton*. We describe the *INTEGRAL* and *XMM-Newton* observations and data reduction in § 2. In § 3 we construct the long-term flux history of IGR J16358–4726 spanning  $\sim 6$  yr and search for evidence of possible orbital modulations; further, we perform a timing analysis using *INTEGRAL* data to identify changes in the observed period. In § 4 we perform both a wide-band joint spectral analysis to better constrain the integrated source spectrum and phase-resolved spectroscopy with *Chandra* to search for spectral variations and

<sup>1</sup> NASA Marshall Space Flight Center, National Space Science and Technology Center, Huntsville, AL.

<sup>2</sup> Universities Space Research Association, Huntsville, AL.

<sup>3</sup> *INTEGRAL* Science Data Centre, Versoix, Switzerland; and Observatoire de Genève, Sauverny, Switzerland.

<sup>4</sup> INAF/Istituto di Astrofisica Spaziale e Fisica Cosmica-Roma, Rome, Italy.

<sup>5</sup> Physics Department, Ben-Gurion University, Be’er-Sheva, Israel.

<sup>6</sup> Sabanci University, FENS, Orhanli-Tuzla, Istanbul, Turkey.

<sup>7</sup> *Spitzer* Science Center, California Institute of Technology, Pasadena, CA.

TABLE 1  
 LOG OF IGR J16358–4726 OBSERVATIONS

Observatory	Start (MJD)	End (MJD)	Revolutions	Exposure <sup>a</sup> (days)
<i>INTEGRAL</i> .....	52,650	52,743	30–60	22.953
	52,859	52,919	100–119	32.944
	53,060	53,084	167–174	10.164
	53,236	53,263	226–234	13.411
<i>Chandra</i> .....	52,722.1691	52,722.4939	...	0.297
	52,750.1484	52,750.7093	...	0.545
<i>XMM-Newton</i> .....	53,051.6064	53,051.9865	...	0.193/0.231/0.205
	53,252.7663	53,253.1255	...	0.263/0.288/0.299
	53,270.6780	53,271.2782	...	... /0.411/0.414

NOTE.—All public and Core Program ISGRI data when IGR J16358–4726 was within the ISGRI PCFOV between 2003 January 11 (Rev 30) and 2004 September 15 (Rev 234) are included.

<sup>a</sup> The net useful exposure times. *INTEGRAL* times reflect ISGRI pointed observations where IGR J16358–4726 fell within the PCFOV. Times from *XMM-Newton* are for the EPIC-PN/MOS1/MOS2 detectors.

features. A discussion of our results and possible models on the nature of the source is presented in § 5.

## 2. OBSERVATIONS AND DATA REDUCTION

### 2.1. *INTEGRAL*

A significant portion of the observing time allocated to the *INTEGRAL* Core Program is dedicated to the study of hard X-ray and  $\gamma$ -ray sources in the Galaxy. This time is mainly divided into Galactic Plane Scans (GPS) and Galactic Center Deep Exposures (GCDE). The observing strategy consists of pointings lasting 2.2 and 1.8 ks for GPS and GCDE, respectively, that are spread in various grid patterns to ensure the best use of the coded-mask instruments. As IGR J16358–4726 is located near the Galactic plane, it has been regularly monitored by *INTEGRAL* (Lutovinov et al. 2005). Hereafter we reference the *INTEGRAL* observations by *revolution* (Rev) number (1 total revolution is completed every  $\sim 3$  days) and by individual *science window* (scw) number (1 scw  $\sim 2$  ks). IGR J16358–4726 was discovered as a transient source in Rev 52 and faded beyond detection a few days later. Since then, no other detection of this source has been reported with *INTEGRAL*.

We have searched the *INTEGRAL* public database to identify additional periods of IGR J16358–4726 activity; our search included all Guest Observer data obtained from the start of the mission until 2003 October 16.3 (MJD 52,928.3), as well as Core Program data obtained until 2004 December 2 (MJD 53,341.1). Our data set comprises four epochs when the Galactic center was deeply observed, resulting in a total exposure time of 4.3 Ms. The average off-axis angle for all IGR J16358–4726 observations is larger than  $10^\circ$ . We have, therefore, only used data taken with the large field-of-view (FOV) coded-mask instrument IBIS/ISGRI (20 keV–1 MeV; Ubertini et al. 2003; Lebrun et al. 2003) on board *INTEGRAL* in this investigation. Table 1 presents the details of the source visibility periods and, for each of them, the fraction of the time when the source was effectively observed in the IBIS partially coded field of view (PCFOV) of  $29^\circ \times 29^\circ$ . Revolutions with net source exposure  $< 1$  ks were discarded since these typically correspond to pointings during which the source crossed the PCFOV far from the center. These omitted revolutions are 56, 61, 63, 164, 169, 179, 183, 241, 243, and 244.

The data from all pointings with the source within the ISGRI PCFOV were reduced with the Offline Scientific Analysis (OSA)

 TABLE 2  
 LOG OF *INTEGRAL* ISGRI OBSERVATIONS WITH DETECTIONS OF IGR J16358–4726

Revolution	Start (MJD)	End (MJD)	Exposure (ks)	$\theta^a$ (deg)	$\sigma_{\text{det}}^b$
052.....	52,717.3972	52,718.7003	77.1	11.4 (6.1–18.2)	44.7
054.....	52,722.2812	52,724.6796	89.6	10.2 (2.5–18)	28.6
055.....	52,725.0607	52,726.4123	90.4	11.3 (5.7–14.3)	16.3
057.....	52,732.5051	52,733.6327	70.5	11.3 (5.7–11.3)	6.1

<sup>a</sup> Average off-axis angle. Numbers in parentheses indicate the range of off-axis angle. Revs 53 and 56 were not considered since the source fell outside the PCFOV.

<sup>b</sup> The detection significance is derived from the mosaicked images for each revolution (20–60 keV).

software<sup>8</sup> (ver. 4.2 and ver. 5.0) provided by the *INTEGRAL* Science Data Center (Courvoisier et al. 2003). This resulted in  $\sim 2000$  science windows distributed between Revs 30 and 234. For each pointing we extracted sky images and then built mosaic images with longer exposures. As the source is a transient, we extracted and inspected light curves from each individual pointing, as well as from the composite images. During the times the source was detected we extracted light curves on shorter timescales of  $\sim 50$  s. We also generated individual spectra for each pointing and then summed them to obtain one average spectrum per revolution where the source was detected. The same technique was used to generate phase-resolved spectra based on the pulse period derived with the ISGRI data. All of the pointings were initially analyzed with OSA 4.2; however, the revolutions in which the source was detected were subsequently reanalyzed with OSA 5.0 (see details in Table 2). Light curves were corrected to the solar system barycenter using the OSA 5.0 barycent tool.

It was practically impossible to observe the source with the X-ray instrument JEM-X, which has an FOV with a diameter of  $13.2^\circ$ ; moreover, it was very difficult to analyze sources lying more than  $3^\circ$  away from the center of the JEM-X FOV. In the single pointing where the source was located  $\sim 2.5^\circ$  from the center (revolution 54), we do not detect it with a  $3\sigma$  upper limit of  $0.005$  counts  $\text{s}^{-1}$ . Finally, data from the third instrument on board *INTEGRAL*, the Gamma Ray Imaging Spectrometer (SPI), were also not analyzed because the instrument angular resolution of  $2^\circ$  is too large for the crowded region where IGR J16358–4726 is located (e.g., 4U 1630–47 is located only  $19'$  away).

### 2.2. *XMM-Newton*

We observed the location of IGR J16358–4726 with *XMM-Newton* starting on 2004 February 15.6 UT and again on 2004 September 4.8 UT for  $\sim 32$  ks in each pointing. The field of IGR J16358–4726 was observed again by *XMM-Newton* during a scheduled observation of SGR 1627–41 on 2004 September 23.3 UT. During the latter observation, the EPIC-PN was operating in Small Window Mode; thus, no PN data of IGR J16358–4726 were collected. IGR J16358–4726 was detected  $9.8'$  off-axis with the MOS detectors during this observation.

The observation data files were processed using the *XMM-Newton* Standard Analysis System (SAS ver. 6.5.0) tools *emchain* and *epchain* and HEASOFT/FTOOLS (ver. 6.0.2). We first identified and removed times of extremely high background rates in the PN and both MOS detectors ( $> 15$  counts  $\text{s}^{-1}$  across the entire detector) and then repeatedly applied a  $3\sigma$  clipping criterion to the 0.5–10.0 keV count rates until all of the remaining events were

<sup>8</sup> Available at <http://isdc.unige.ch/>.

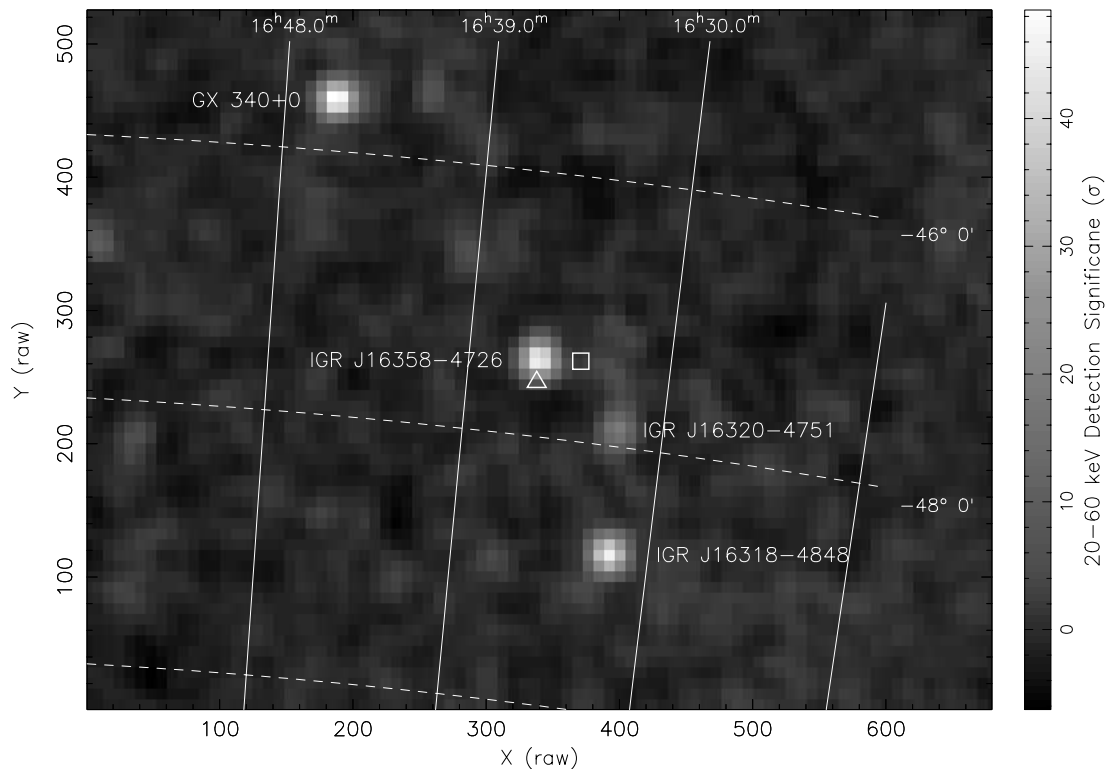


FIG. 1.—*INTEGRAL* IBIS/ISGRI (20–60 keV) image of the field containing IGR J16358–4726 taken on 2003 March 19 (Rev 52). The source detection was significant at the  $44.7\sigma$  level in 77.1 ks of useful exposure time. Sources detected in this portion of the sky are labeled in the image, and the locations of SGR 1627–41 (*triangle*) and 4U 1630–47 (*square*) are also identified. The latter two sources are not detected above 20 keV during this revolution. For reference, the image pixel size is  $4.9''$  on a side. [See the electronic edition of the *Journal* for a color version of this figure.]

within  $\pm 3\sigma$  of the mean rate. The remaining useful exposure times are given in Table 1.

For the first two observations, when the source was detectable and imaged on-axis, we extracted source spectra from each detector using an extraction radius of  $r = 18''$ ; we used  $r = 30''$  in the third observation when IGR J16358–4726 was imaged off-axis. We then built instrument response files using the standard SAS tools *arfgen* and *rmfgen*. Background spectra were collected using offset regions close to the source location for each observation with a total area 15 times the source region. Finally, we grouped spectral bins to obtain at least 15 counts  $\text{bin}^{-1}$  before background subtraction in each spectrum.

We extracted events centered on the *Chandra* source location from the first *XMM-Newton* PN observation; the source was not detected. Using *WebPimms* and assuming the *Chandra* spectral model ( $\Gamma = 0.8$ ,  $\log N_{\text{H}} = 23.3$ ; Patel et al. 2004), we derived a  $3\sigma$  upper limit on the 1–10 keV unabsorbed flux of  $5.4 \times 10^{-14}$  ergs  $\text{cm}^{-2} \text{s}^{-1}$ . The limits derived from the MOS detectors are consistent with but not more constraining than the PN measurement. During the second *XMM-Newton* observation we clearly detected a source at the location of IGR J16358–4726 with an average total PN count rate of  $(1.78 \pm 0.09) \times 10^{-2}$  counts  $\text{s}^{-1}$  (1–10 keV). We estimated a PN background rate of  $(0.31 \pm 0.01) \times 10^{-2}$  counts  $\text{s}^{-1}$ . For the MOS1 and MOS2 detectors we found total rates of  $(5.5 \pm 0.5) \times 10^{-3}$  and  $(6.0 \pm 0.5) \times 10^{-3}$  counts  $\text{s}^{-1}$  and calculated background rates of  $(1.06 \pm 0.03) \times 10^{-3}$  and  $(1.53 \pm 0.04) \times 10^{-3}$  counts  $\text{s}^{-1}$ , respectively. Source and background spectra were also extracted from the off-axis data from the final *XMM-Newton* observation. The MOS detectors clearly detect the source with total and background rates of  $(6.9 \pm 0.4) \times 10^{-3}$  and  $(2.89 \pm 0.07) \times 10^{-3}$  counts  $\text{s}^{-1}$  for MOS1 and  $(6.1 \pm 0.4) \times 10^{-3}$  and  $(3.74 \pm 0.08) \times 10^{-3}$  counts  $\text{s}^{-1}$

for MOS2. However, the poor quality of the MOS spectra in this observation did not allow for useful spectral analysis.

## 3. RESULTS

### 3.1. Source Position

IGR J16358–4726 was brightest during revolution 52 with an average count rate of  $5.8 \pm 0.1$  counts  $\text{s}^{-1}$  and a detection significance of  $44.7\sigma$  (Fig. 1; 20–60 keV). We used a mosaic of that epoch to extract the *INTEGRAL* best source position at R.A. =  $16^{\text{h}}35^{\text{m}}52.5^{\text{s}}$  and decl. =  $-47^{\circ}25'16''$  (J2000.0) with an uncertainty of  $20''$  that includes a  $10''$  systematic error due to instrument misalignment. An additional systematic error (proportional to the source significance) of  $44''$  is also present from the image reconstruction (Gros et al. 2003). This position is consistent with the location initially reported by Kouveliotou et al. (2003a). A more accurate location using the second *XMM-Newton* observation and the initial *Chandra* observations is presented in a companion paper by S. Wachter et al. (2007, in preparation) together with a discussion on the results of our search for an infrared counterpart for IGR J16358–4726.

### 3.2. Source X-Ray Light Curve

Figure 2 exhibits the ISGRI light curve of IGR J16358–4726 during the 2003 March outburst of the source (Revs 52–55, spanning a total of 9 days). The gaps in the figure correspond to Revs 53 and 56, when the source was outside the IBIS PCFOV. During the source maximum (Rev 52) the average ISGRI count rate was  $5.8 \pm 0.1$  counts  $\text{s}^{-1}$ , corresponding to 36 mcrab. The initial peak lasted less than 2 days; the source flux fell to 3.2 counts  $\text{s}^{-1}$  (20 mcrab) during the following 8 days and beyond detection level  $< 1$  count  $\text{s}^{-1}$  ( $\lesssim 7$  mcrab) after Rev 57.

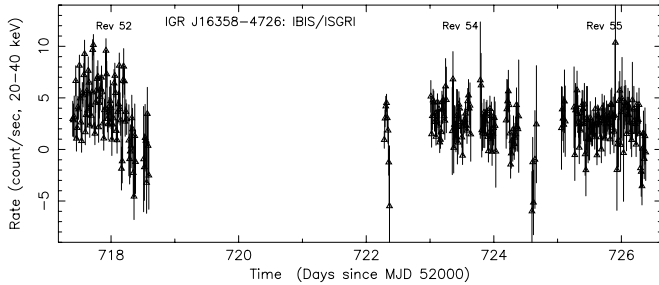


FIG. 2.—ISGRI light curve of IGR J16358–4726 (20–45 keV) integrated in time bins of 1000 s, starting on 2003 March 19 and spanning  $\sim 9$  days. Revs 53 and 56 were not used in this plot because the source fell outside the IBIS PCFOV (see also text and Table 2). The dashed lines indicate the time interval of the initial 26 ks *Chandra* observation.

The long-term flux history of IGR J16358–4726 (unabsorbed 2–10 keV) spanning  $\sim 6$  yr was constructed by using all available pointed observations of the source and is presented in Figure 3. The archival source flux measurements with *ASCA* and *BeppoSAX* prior to the 2003 outburst were originally presented in Patel et al. (2004). The 2–10 keV flux was estimated for each X-ray instrument by assuming a spectrum similar to the one measured with *Chandra* in 2003. The *INTEGRAL* flux was extrapolated using the best-fit spectral model to the ISGRI data during the outburst (Rev 52). Using the extrapolated *INTEGRAL* discovery flux and the two *Chandra* flux measurements, we find that the outburst light curve decays as an exponential with an  $e$ -folding time of  $9.2 \pm 0.6$  days. The *RXTE* observation of IGR J16358–4726 is complicated by significant X-ray emission from the Galactic ridge. Using spectral fits obtained after modeling and subtracting the Galactic ridge component (Revnivtsev 2003), we estimate an unabsorbed 2–10 keV flux of  $2.9 \times 10^{-10}$  ergs  $\text{cm}^{-2}$   $\text{s}^{-1}$  on MJD 52,724.4. This flux is nearly a factor of 2 larger than the flux we derive from our *Chandra* measurement on MJD 52,722.3. Such a large change in the source flux is difficult to reconcile with the constant average rate observed during the 7.1 hr *Chandra* observation. This data point has been omitted from Figure 3 for clarity. The corresponding 2–10 keV luminosities in Figure 3 were then determined by assuming an average source distance of 7 kpc.

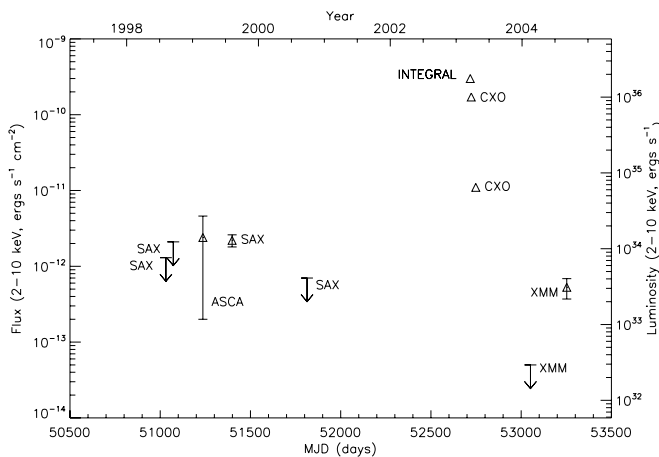


FIG. 3.—Unabsorbed X-ray flux history of IGR J16358–4726; upper limits at the 90% significance level are indicated for three *BeppoSAX* measurements and one *XMM-Newton* measurement. The fluxes (left side of  $y$ -axis) derived from the *INTEGRAL* data are extrapolated into the 2–10 keV energy range using the best joint *Chandra-INTeGRAL* spectral fit for Rev 52. The luminosities (right side of  $y$ -axis) were calculated assuming an average distance of 7 kpc for the source.

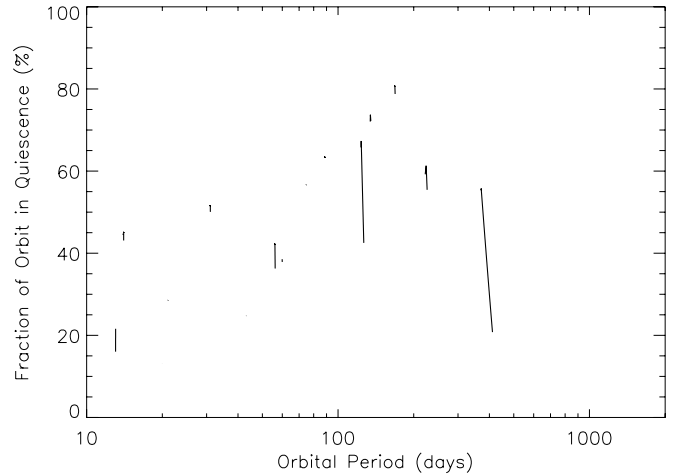


FIG. 4.—Maximum duration of the quiescent orbital interval for possible orbital periods of the IGR J16358–4726 system. Only the periods are shown, where the orbit could be divided into an active phase region (containing all of the detections) and a quiescent phase region (containing all of the nondetections).

The detections and nondetections of IGR J16358–4726 shown in Figure 3 motivated a search for orbital periods based on the assumption that this system exhibits a behavior similar to the largest class of known transient accreting pulsars, those with Be (or Oe) star companions. These systems often have series of outbursts separated by their orbital period, with the outbursts occurring near periastron passage in an eccentric orbit (Bildsten et al. 1997). For each one of a finely spaced grid of trial orbital periods in the range of 10–2000 days, an attempt was made to divide the orbit into an active phase region (containing all of the detections) and a quiescent phase region (with all of the nondetections). Each time such a phase segregation was possible, it was considered as a candidate period. Figure 4 shows the duration of the longest possible quiescent orbital phase region for each candidate period. Note that no candidate periods longer than  $\sim 400$  days were found. Thus, although the search did not identify any unique orbital period, it did demonstrate that a (yet undiscovered) periodic outbursting could be occurring in intervals of at most 1 yr.

### 3.3. Timing Analysis

We searched for all detections of IGR J16358–4726 in the public, 2 yr long IBIS/ISGRI database (see also § 2) in two energy ranges: 20–60 keV and 60–150 keV. We then built mosaic images for each revolution and extracted light curves at each energy band where the net exposures (at the source location) were higher than 5 ks, for better statistics. At no time was the source detected above 60 keV. Whenever the source was not detected in one revolution (typical  $3\sigma$  flux upper limits of  $\sim 0.3$  counts  $\text{s}^{-1}$ ), we grouped adjacent revolutions to increase sensitivity. The final net exposure times for the four resulting detection revolutions and their dates are given in Table 2.

Initially, we generated Lomb-Scargle periodograms (Scargle 1982) from the ISGRI light curves with the higher count rate detections (Revs 52, 54, and 55; Fig. 2) and clearly detected significant modulations at  $\sim 1.65$  hr (as well as its first harmonic). Further, we divided the light curve into two sections (Rev 52 and Revs 54+55) to search for changes in modulation frequency. Although we detected significant pulsations in the initial portion of the light curve (until  $\sim 7 \times 10^4$  s after detection) with a period of  $5970 \pm 15$  s, in the latter portion of the light curve we found moderate evidence for pulsations consistent with the previously measured frequency. In both orbit segments we detected significant

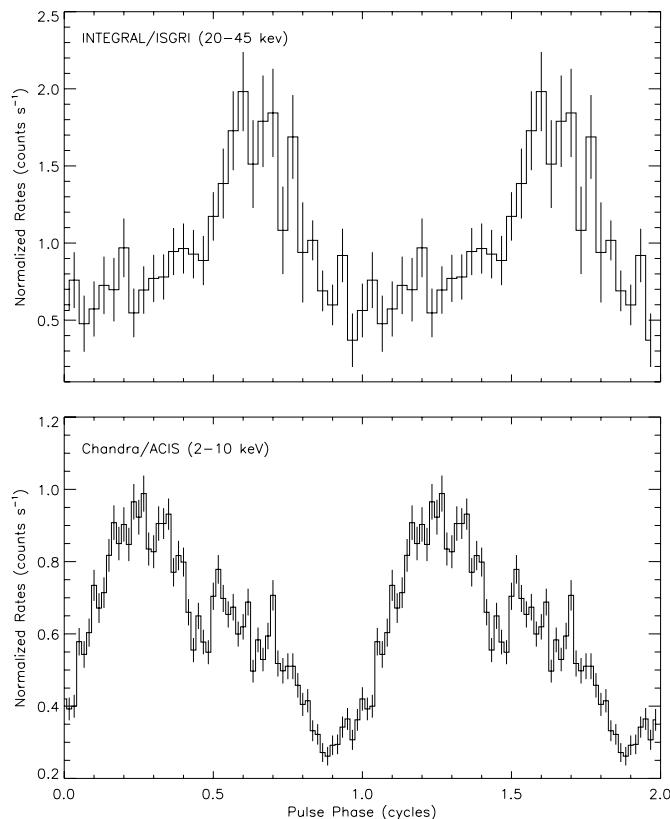


FIG. 5.—*Top*: *INTEGRAL* ISGRI pulse profile (20–45 keV) folded with a period  $P = 5965 \pm 15$  s. *Bottom*: *Chandra* ACIS (2–10 keV) pulse profile folded with the same period. Both profiles are referenced to the same date (MJD 52,700). The *Chandra* data were acquired  $\sim 5$  days after the ISGRI detection.

power in the  $\sim 3000$  s harmonic. However, due to the poor statistics during the second ISGRI interval, we were unable to conclusively determine pulse period changes exclusively within these data using the Lomb-Scargle method. Finally, we proceeded into folding the first  $\sim 10^5$  s of the ISGRI light curve on the best determined *INTEGRAL* period (Fig. 5) and compared it with the *Chandra* X-ray light curve acquired on 2003 March 24 folded on the same ephemeris. There appears to be evidence of a phase shift between these two profiles suggesting evolution of the pulse profile or period over a few days; however, we caution that since the profiles are in different energy bands, this shift could be due to spectral evolution.

In the following we describe a more detailed method for the determination of the pulse ephemeris. We again determine the pulse periods separately from the data in Rev 52 and Revs 55+54 combined using a method that takes into consideration the properties of the data quality and the observation windows. An important aspect of this analysis was the need to correctly account for the data gaps and the large variations in rate errors, which occurred in both of these intervals. These gaps and variations were due to changes in pointing directions during the observations, causing missing data when the source was outside the coded FOV and increasing the errors as the source moved outward within the PCFOV. For this purpose only exposure-corrected count rates in the 20–45 keV energy band with 50 s time resolution were analyzed.

We first determined the pulse periods using a technique based on  $\chi^2$  fits of the rates. To account for the gradual decrease in flux during the observations, the rates in each interval were fitted to separate linear trends, and the rates were then divided by the fit. The trend amounted to 1.0% in Rev 52 and 31% over the course

of Revs 54+55. For a grid of trial pulse periods ranging from 5000 to 7000 s, the normalized rates were then fitted to a model consisting of a repeated pulse profile, parameterized by a Fourier expansion limited to constant, fundamental, and first harmonic terms. Most of the power of the pulse was found to be in the fundamental and first harmonic, so we did not include higher harmonics. The improvement in this fit ( $\Delta\chi^2$ ) over a fit of the normalized rates to a constant is shown versus the period in Figure 6 for both time intervals. This  $\Delta\chi^2$  is equivalent to the  $Z_2^2$  statistic (Buccheri et al. 1983) in the case of uniformly spaced data with uniform errors and periods much smaller than the duration of the observation. The best-fitted periods were  $P = 5964.7 \pm 12.1$  s (Rev 52) and  $P = 5870.9 \pm 3.4$  s (Revs 54+55), where the errors include only counting statistics.

To check these results and to quantify any noise in excess of counting statistics, each analysis interval was divided into sub-intervals and the pulse profile for each subinterval was obtained by fitting the rates with a second-order Fourier expansion pulse profile model, with the period fixed to that determined above for that interval. These were then cross-correlated with the mean profile for the full interval to obtain pulse phase measurements. The deviation of these phases from those expected from the estimated period is shown in Figure 7. Using linear fits to the pulse phases, we obtained pulse period estimates of  $P = 5964.9 \pm 12.2$  s for Rev 52 and  $P = 5871.3 \pm 3.3$  s for Revs 54+55 combined, consistent with the previous results. The  $\chi^2$  of these fits is 4.72 and 3.47, respectively (both with 3 degrees of freedom). These results are summarized in Table 3 with the errors increased by the square root of the reduced  $\chi^2$  to account for any noise in excess of counting statistics.

In Figure 8 we show the evolution of the IGR J16358–4726 pulse periods. The two *Chandra* measurements agree with the second ISGRI measurements (Revs 54+55), but the initial ISGRI period (Rev 52) is significantly higher than the others. The 94 s difference between the first and second ISGRI periods is significant at the  $6\sigma$  level. If this difference is due to a gradual change in the spin period of a neutron star, the mean spin period derivative between the measurements is  $(-1.65 \pm 0.28) \times 10^{-4}$ . The last *Chandra* measurement indicates that this putative spin-up trend may have ended. Unfortunately, the Rev 54+55 data only weakly constrain period changes; fitting the pulse phases in Revs 54+55 with a quadratic results in the estimate of  $\dot{P} = (1.9 \pm 1.1) \times 10^{-4}$ . Over the 18.8 pulse cycles that occur during Rev 52, the 94 s difference in period amounts to only 1760 s or 0.30 pulse cycles of phase difference. It could be possible that the pulse profile, which our analyses assume is constant, has changed sufficiently to cause such an apparent phase shift. Figure 9 shows the 20–45 keV ISGRI rates epoch-folded with a 5965 s period, for the five subintervals of Rev 52 used in Figure 7. Also shown on the profile is the position of the phase reference that would have resulted if the profiles were folded with a period of 5871.3 s. Examining these alternate phase alignments of pulse profiles, we conclude that this period difference is most likely not due to profile changes.

We have also determined a pulse period using the *XMM-Newton* EPIC-PN observation from 2004 September; in all other data sets the source was too faint to detect pulsations. We correct the photon times of arrival in the events list to the solar system barycenter and extract all events between 0.5 and 10.0 keV from a slightly smaller extraction region ( $12''$ ) as was used in the spectral analysis (see also § 4). We performed a  $Z_2^2$  test on periods ranging from 4000 to 7000 s and clearly detected the pulsation in the EPIC-PN light curve with a period of  $P = 5858 \pm 74$  s. This period is consistent with those measured using *Chandra* and

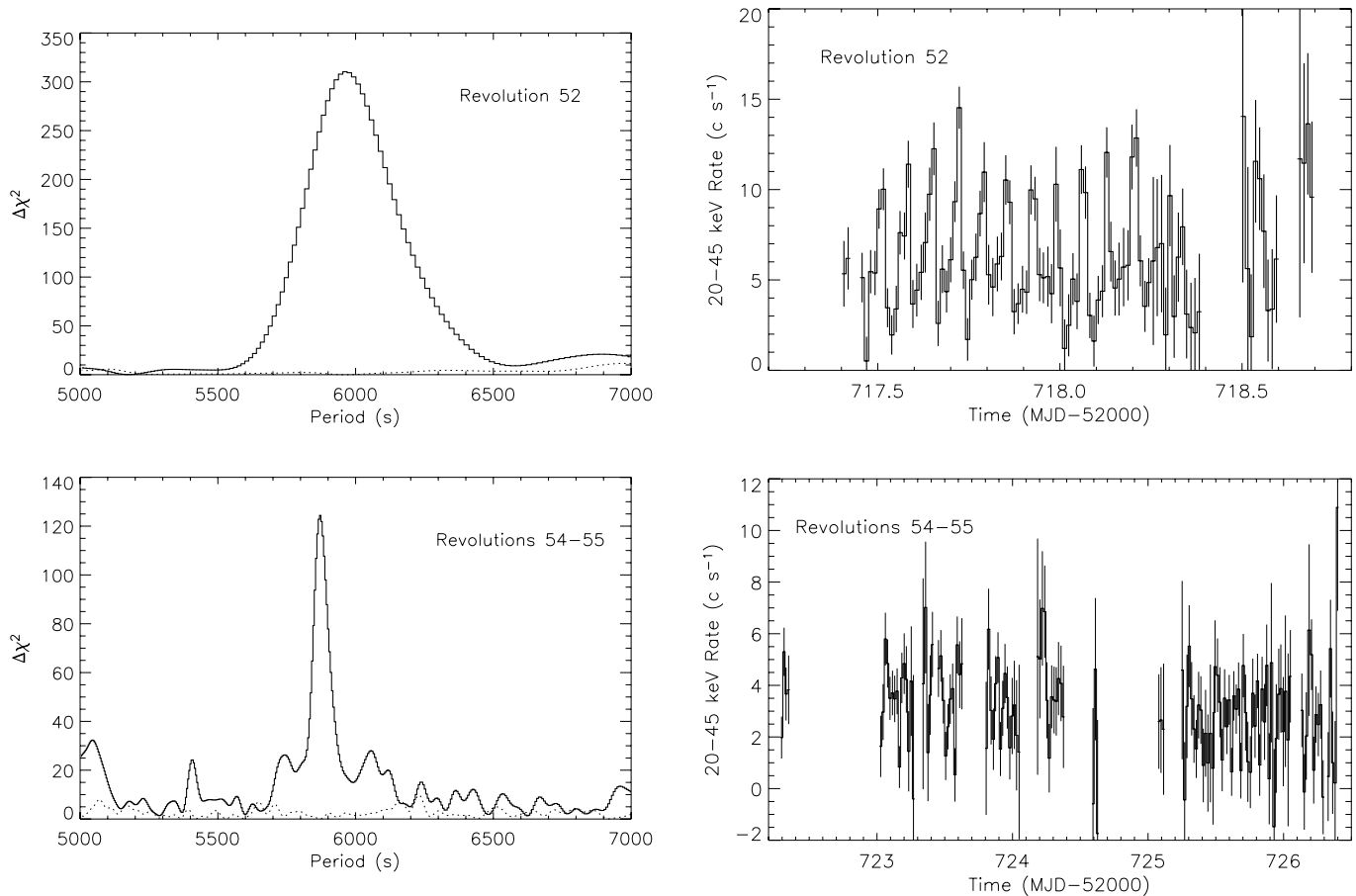


FIG. 6.—Decrease in  $\chi^2$  between a fit of the normalized rates to a constant and a second-order Fourier expansion pulse profile vs. period (*solid line*) for the ISGRI data in Rev 52 (*top*) and Revs 54+55 combined (*bottom*). Also shown (*dotted lines*) is the same statistic after the best-fitted profile (at the peak  $\Delta\chi^2$  period) was subtracted from the normalized rates. This shows that most of the power away from the main peak is caused by the pulsations at the peak  $\Delta\chi^2$  period.

*INTEGRAL* in 2003. We present the folded PN light curve in Figure 10.

#### 4. SPECTRAL ANALYSIS

##### 4.1. *INTEGRAL* ISGRI plus *Chandra* ACIS-S Spectral Analysis

The phase-averaged spectral fit results from the *Chandra* data alone have already been presented in Patel et al. (2004). We have therefore initially fitted a power-law model to the *INTEGRAL* ISGRI 20–200 keV spectrum, which resulted in an unacceptable fit ( $\chi^2/\nu = 79/9$ ). A thermal blackbody (BB) model resulted in a better fit ( $\chi^2/\nu = 13.7/9$ ) with  $kT_{\text{BB}} = 6.2 \pm 0.1$  keV; however, the resulting BB source radius was only 0.15 km (assuming a source distance of 7 kpc). Subsequently, we jointly fitted the phase-averaged spectra measured with ISGRI and the initial *Chandra* observation, to better characterize the IGR J16358–4726 spectrum in outburst. Since these data were collected at slightly different times, we allowed the model normalizations between data sets to be free and linked all other spectral parameters. The data were well fitted by a Comptonization model (Titarchuk 1994) with the best-fit parameters given in Table 4. For comparisons to power-law models typically used in the lower X-ray bands, we have also modeled the spectrum using an absorbed power-law model with a high-energy exponential cutoff (Table 4).

On 2003 March 24, we were fortunate to have simultaneous *INTEGRAL* and *Chandra* observations, providing us with the only broadband high-energy spectral coverage for IGR J16358–4726 to date. The *INTEGRAL* data available during the time of the

*Chandra* observations consist of four science windows, from which we were able to extract  $\sim 4600$  s of useful exposure time. The light curves from these observations are shown in Figure 11; the overall shape of the ISGRI light curve is consistent with the shape of the *Chandra* light curve during the same time interval, suggesting no evolution in the hard X-ray ephemeris. We performed joint phase-averaged spectroscopy using these simultaneous observations covering approximately one entire pulse (Fig. 11). The data are well represented by a Comptonization model with a Gaussian line feature at 6.4 keV. The best-fit parameters are given in Table 4 and the resulting spectrum is shown in Figure 12.

##### 4.2. *XMM-Newton* EPIC-PN Spectral Analysis

We employed standard  $\chi^2$  methods in obtaining the best fit to the *XMM-Newton* spectral data and analyzed the spectra using the XSPEC (ver. 11.3.21) spectral fitting package (Arnaud 1996). When fitting the MOS and PN spectra simultaneously, we linked the model parameters. However, since the relative flux calibration of these instruments is somewhat uncertain, we allowed the individual normalizations to be free to obtain their best-fit value. We fitted the MOS and PN (0.5–10.0 keV) spectra jointly to a power law and again to a thermal BB model. We accounted for absorption due to intervening gas and dust from the Galaxy using the Tuebingen-Boulder interstellar medium absorption model (XSPEC model *tbabs*) with the relative abundances and cross sections from Wilms et al. (2000) and with He cross section from Yan et al. (1998). An acceptable fit ( $\chi^2/\nu = 30.3/38$ ) resulted when the data were modeled with the power law with a best-fit spectral index

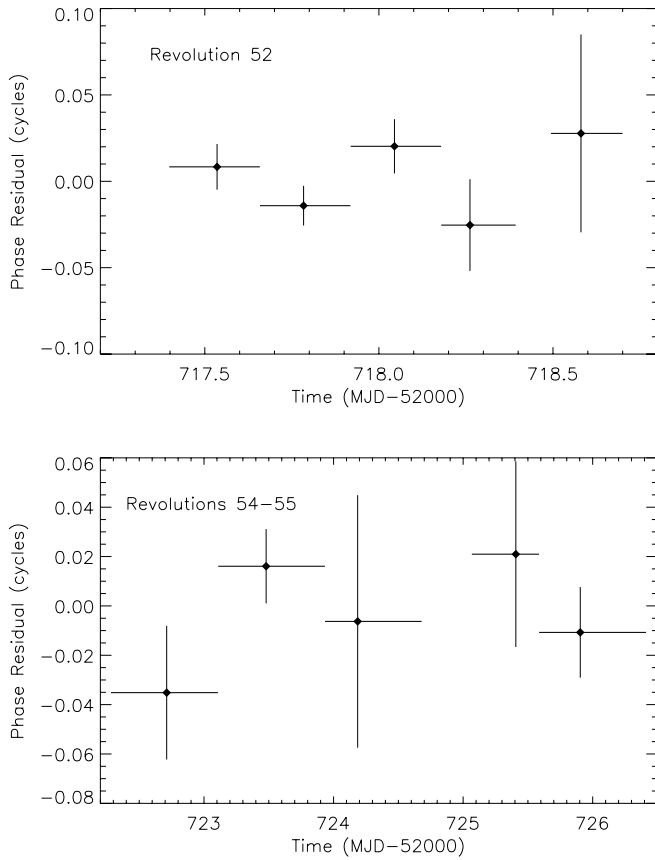


FIG. 7.—Phase offsets of the pulse profiles from subintervals of Rev 52 (*top*) and Revs 54+55 combined (*bottom*) relative to phase ephemerides with constant periods of 5964.7 and 5870.9 s, respectively.

$\Gamma = 1.1_{-0.3}^{+0.4}$  and column density  $N_{\text{H}} = 18_{-3}^{+4} \times 10^{22} \text{ cm}^{-2}$ . The unabsorbed (1–10 keV) flux measured from this model was  $7.1 \times 10^{-13} \text{ ergs s}^{-1} \text{ cm}^{-2}$ . A fit using a BB model resulted in a nearly identical quality fit ( $\chi^2/\nu = 30.4/38$ ) with  $kT_{\text{BB}} = 2.3_{-0.2}^{+0.6} \text{ keV}$  and  $N_{\text{H}} = (14 \pm 3) \times 10^{22} \text{ cm}^{-2}$ . The unabsorbed (1–10 keV) flux measured for this model was  $4.9 \times 10^{-13} \text{ ergs s}^{-1} \text{ cm}^{-2}$ .

To test the goodness of the  $\chi^2$  fitting, we also fitted the unbinned data using the  $C$ -statistic (Cash 1979) and again using the grouped data and the  $\chi^2$  fitting with the weighting method described by Churazov et al. (1996) as implemented in XSPEC, and we found consistent results.

#### 4.2.1. Phase-resolved Spectroscopy

We have extracted 10 individual phase-resolved spectra from the *Chandra* ACIS observation of 2003 March. We simultaneously fitted the spectra using an absorbed power-law plus Gaussian line model. The model consists of six parameters for each spectrum (the equivalent hydrogen column  $N_{\text{H}}$ , spectral power-law index  $\Gamma$ , power-law normalization PLNORM, Gaussian line centroid en-

TABLE 3  
PULSE PERIODS DETERMINED FROM ISGRI DATA

Revolutions	Epoch <sup>a</sup> (MJD)	Period (s)	Error (s)
52.....	52,717.84	5965	15
54–55.....	52,724.39	5871.3	3.5

<sup>a</sup> The weighted mean of the observation times using the inverse square rate errors as weights.

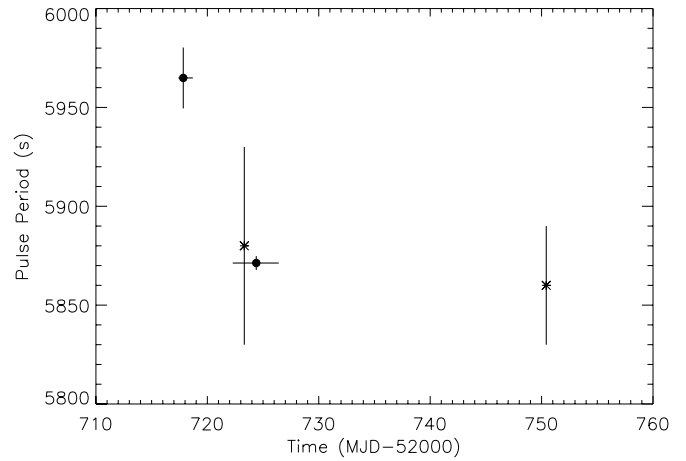


FIG. 8.—Pulse periods determined from the ISGRI data (*filled circles*) along with the measurements based on *Chandra* observations (*asterisks*).

ergy  $E_{\text{line}}$ , width  $\sigma_{\text{line}}$ , and flux  $F_{\text{line}}$ ) for a total of 60 parameters. For all fits we allow PLNORM for each spectral model to acquire its best-fit value (i.e., PLNORM is *free* and *unlinked*). All of the remaining parameters were forced to have the same value (i.e., were *linked*) for each spectrum and each parameter was free to acquire its best-fit value. This fit results in a statically acceptable fit with  $\chi^2/\nu = 562.6/542$  and best-fit model parameters of  $N_{\text{H}} = (3.5 \pm 0.1) \times 10^{23} \text{ cm}^{-2}$ ,  $\Gamma = 0.59 \pm 0.09$ ,  $E_{\text{line}} = 6.38 \pm 0.01 \text{ keV}$ ,  $\sigma_{\text{line}} = 54 \pm 18 \text{ eV}$ , and  $F_{\text{line}} = (2.6 \pm 0.3) \times 10^{-12} \text{ ergs cm}^{-2} \text{ s}^{-1}$ .

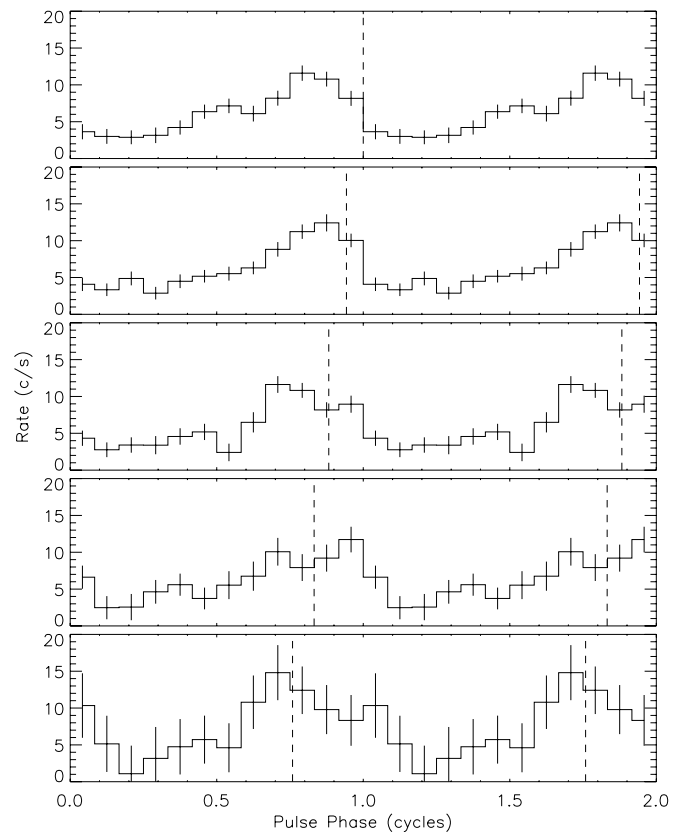


FIG. 9.—Pulse profiles for five subintervals in Rev 52 obtained by epoch-folding the 20–45 keV rates at a period of 5965 s. The dashed lines show the location of phase zero that would have resulted if the rates were folded with the 5871.3 s period determined for Revs 54+55.

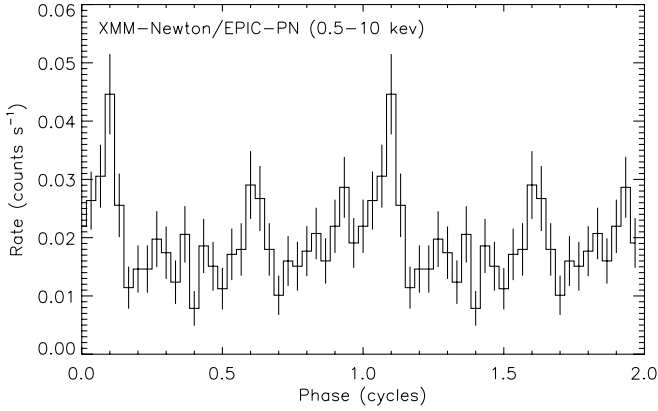


FIG. 10.—Folded *XMM-Newton* EPIC-PN pulse profile (0.5–10 keV) with period  $P = 5858 \pm 74$  s measured in 2004 September and referenced to the same epoch as in Fig. 5.

To search for variations with phase of the linked parameters, we first unlinked the  $N_{\text{H}}$  while continuing to hold the others linked. This resulted in significant improvements in the fit with  $\Delta\chi^2 = 29.1$  with an  $F$ -test probability of  $F_{\text{prob}} = 0.0011$ . We next unlinked  $\Gamma$  and found an additional improvement of  $\Delta\chi^2 = 21.9$ . To test whether variations in  $\Gamma$  or  $N_{\text{H}}$  (or both) were responsible for the majority of the fit improvement, we repeated the same test, this time first unlinking  $\Gamma$ . When unlinking only  $\Gamma$ , we find a  $\Delta\chi^2 = 41.8$  with  $F_{\text{prob}} = 7.5 \times 10^{-6}$ . Unlinking  $N_{\text{H}}$  at this point negligibly improves the fit with an additional  $\Delta\chi^2 = 9.5$ . There is

TABLE 4  
*INTEGRAL* AND *Chandra* JOINT SPECTRAL FIT RESULTS

Parameter	Value <sup>a</sup>	Value <sup>b</sup>
Model 1: Absorbed Comptonization plus Gaussian		
$N_{\text{H}}$ ( $\times 10^{22}$ cm <sup>-2</sup> )	$27.9 \pm 0.9$	$36 \pm 2$
$E_{\text{line}}$ (keV)	$6.39 \pm 0.01$	$6.38 \pm 0.02$
$\sigma$ (keV)	$0.07 \pm 0.02$	$0.06^{+0.03}_{-0.06}$
$kT_{\text{injection}}$ (keV)	$2.1 \pm 0.1$	$0.4^{+3.3}_{-0.4}$
$kT_{\text{plasma}}$ (keV)	$7.9 \pm 0.6$	$8.2 \pm 0.5$
$\tau$	$3.8 \pm 0.7$	$9.5 \pm 1.1$
$F_{\text{line}}$ ( $\times 10^{-12}$ ergs cm <sup>-2</sup> s <sup>-1</sup> )	$2.7 \pm 0.03$	$3.3 \pm 0.7$
$F_{2-10 \text{ keV}}^c$ ( $\times 10^{-10}$ ergs cm <sup>-2</sup> s <sup>-1</sup> )	$1.37^{+0.05}_{-0.08}$	$1.8^{+1.7}_{-0.4}$
$R_{\text{ACIS/ISGRI}}^d$	0.45	1
$\chi^2/\nu$	352.0/324	140.5/120
Model 2: Absorbed Power Law with High-Energy Cutoff plus Gaussian		
$N_{\text{H}}$ ( $\times 10^{22}$ cm <sup>-2</sup> )	$33 \pm 1$	$34 \pm 2$
$E_{\text{line}}$ (keV)	$6.39 \pm 0.01$	$6.39 \pm 0.02$
$\sigma$ (keV)	$0.07 \pm 0.02$	$0.06^{+0.3}_{-0.6}$
$\Gamma$	$0.53 \pm 0.08$	$0.39^{+0.1}_{-0.08}$
$E_{\text{cut}}$ (keV)	$19^{+1}_{-2}$	$23 \pm 3$
$E_{\text{fold}}$ (keV)	$12.2 \pm 0.6$	$16 \pm 2.0$
$F_{\text{line}}$ ( $\times 10^{-12}$ ergs cm <sup>-2</sup> s <sup>-1</sup> )	$2.9 \pm 0.03$	$3.2 \pm 0.7$
$F_{2-10 \text{ keV}}^c$ ( $\times 10^{-10}$ ergs cm <sup>-2</sup> s <sup>-1</sup> )	$1.71^{+0.02}_{-0.09}$	$1.62^{+0.04}_{-0.38}$
$R_{\text{ACIS/ISGRI}}^d$	1.12	1
$\chi^2/\nu$	361/324	140.5/120

<sup>a</sup> Fit results derived using all useful ISGRI and ACIS data. Errors reflect the  $1 \sigma$  uncertainty.

<sup>b</sup> Fit results derived using  $\sim 4.6$  ks of ISGRI and ACIS data collected concurrently. Errors reflect the  $1 \sigma$  uncertainty.

<sup>c</sup> Unabsorbed flux derived from the ACIS spectra.

<sup>d</sup>  $R$  is the ratio of the normalizations of the primary model component derived from the ACIS and ISGRI spectra. The model normalizations for both data sets are forced to be linked for fits to the data collected concurrently.

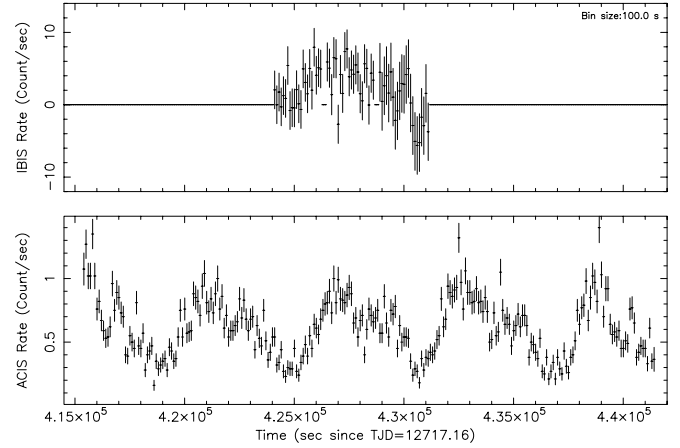


FIG. 11.—Simultaneous *Chandra* ACIS-S2 (2–10 keV) and *INTEGRAL* ISGRI (20–40 keV) light curve of IGR J16358–4726.

clear evidence for change of spectral index with phase with the spectral index ranging from  $\sim 0.1$  to  $0.9$ . Figure 13 shows the pulse profile and the evolution of the power-law index; the spectrum is harder during the peak of the pulse and softens as the rate declines. We conclude that the evidence for varying column density with phase during this observation is marginal at best.

We note that in Patel et al. (2004) we reported a significant decrease in the measured  $N_{\text{H}}$  (by  $\sim 40\%$ ) between this *Chandra* pointing and the one 27 days later. In subsequent spectral fits the power-law index remains unlinked.

The emission line at 6.4 keV is most likely due to Fe fluorescent emission. We tested for variation in the 6.4 keV line parameters using a similar strategy. We performed a series of fits of the spectra after unlinking each line parameter while holding the remaining parameters linked and also performed a fit with all line parameters unlinked. In all cases the improvement in the spectral fits was not significant ( $\Delta\chi^2 < 8$  for nine additional parameters). We find no evidence for evolution of the line with pulse phase.

Finally, we searched the individual spectra for additional line features. The most significant linelike feature in a single spectrum occurred during phase 0.2–0.3 and appeared as a marginally significant emission-line feature at 7.0 keV ( $\Delta\chi^2 = 14.5$  for two additional free parameters and width fixed at  $\sigma_{\text{line2}} = 50$  eV).

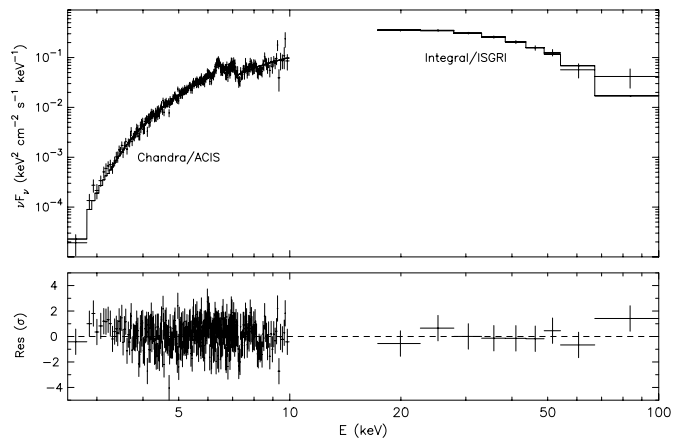


FIG. 12.—Joint *Chandra* ACIS-S2 and *INTEGRAL* ISGRI  $\nu F_{\nu}$  spectrum of IGR J16358–4726 during outburst on 2003 March 24. A highly absorbed Comptonization model gives the best fit to the data. An Fe  $K\alpha$  line feature clearly seen at 6.4 keV during the March 24 observation had faded below the detection capability of *Chandra* during the second observation on 2003 April 21 (Patel et al. 2004). The residuals to the best fit reported in Table 4 are shown in the bottom panel.



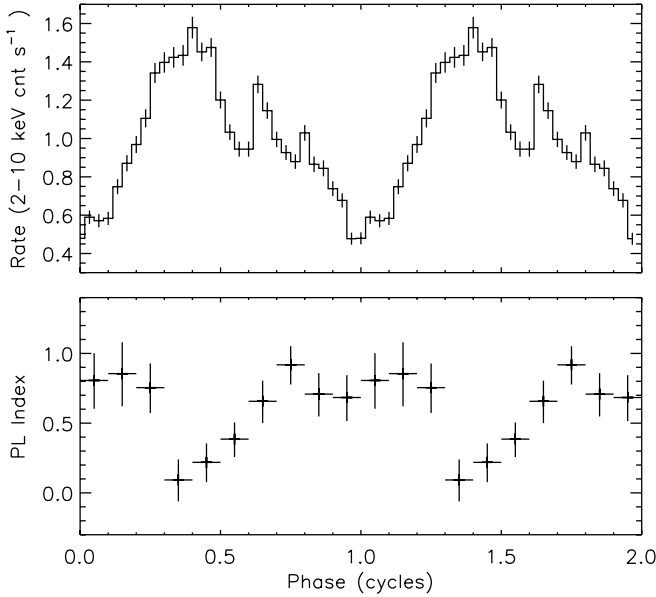


FIG. 13.—Phase-resolved spectral fit results derived with *Chandra* ACIS-S2 (2.0–10.0 keV) data of IGR J16358–4726 in outburst on 2003 March 24. The top panel shows the 2–10 keV observed pulse profile (with 30 phase bins), and the bottom panel shows the spectral power-law index as a function of pulse phase (in 10 phase bins). There is evidence for evolution in the spectral index with the hardest spectra occurring near the end of the pulse rise and a clear spectral softening during the pulse decline.

However, when we considered the number of spectral phase bins searched, we concluded that the line was not statistically significant with a probability of chance occurrence of  $>50\%$ .

## 5. DISCUSSION

There are two feasible origins for the pulsations observed in the flux of IGR J16358–4726: binary orbital modulation or neutron star spin modulation. Given the substantial difference of the period measured in Rev 52 of the *INTEGRAL* data from all later measurements and the expected stability of an orbital period, we must either reject the Rev 52 measurement as unrepresentative of the intrinsic period or reject the orbital modulation hypothesis. It is also possible that pulse shape evolution during Rev 52 could have resulted in this discrepant period; however, this evolution would need to mimic a gradual shifting in phase by 30% of a cycle over the course of the observation. It is not clear how this could be explained in the context of an orbital modulation. Finally, attributing the 1.65 hr modulation to an orbital period would presumably imply that the object is an LMXB, making the nature of the source difficult to reconcile with its unusually hard spectrum.

Assuming that the pulsations are spin induced, there are two possible explanations for the change in spin period between the first observation and the following observations: either the neutron star was spun up by accretion-induced torques, or the neutron star had a glitch in spin period, analogous to those seen in rotation-powered pulsars.

We first consider a scenario where the observed modulation is the neutron star spin and the abrupt change in the frequency is attributed to the sudden transfer of angular momentum between the superfluid interior and the pulsar crust (i.e., a “glitch;” Anderson & Itoh 1975; Ruderman 1976; Alpar 1977). We measure a change of frequency of  $\Delta\nu = 2.7 \pm 0.4 \mu\text{Hz}$  and thus a fractional change in the frequency of  $\Delta\nu/\nu = 1.6 \times 10^{-2}$ . This is  $\sim 10^4$  times larger than the values derived from large glitches reported from radio pulsars (e.g., Shemar & Lyne 1996; Krawczyk et al. 2003) and

anomalous X-ray pulsars, which have typical  $\Delta\nu/\nu \sim 10^{-6}$  (Heyl & Hernquist 1999; Kaspi et al. 2000, 2003; Morii et al. 2005). To date, there has been only one substantiated report of a glitch observed from an accreting pulsar (KS 1947+300, Be system; Galloway et al. 2004). The fractional change in frequency measured in the KS 1947+300 glitch was  $3.7 \times 10^{-5}$ , also significantly larger than those seen in radio or anomalous X-ray pulsars, but still much smaller than observed in IGR J16358–4726. We conclude, therefore, that unless the source underwent a unique and new type of glitch, never observed before, we can exclude this phenomenon as the cause of the neutron star spin variation.

In the following scenario we now assume that the neutron star is fed by an accretion disk during the outburst observed by *INTEGRAL*. Then from the measured spin-up rate and flux and an assumed distance,  $d$ , we can determine the pulsars’ magnetic moment. If instead the pulsar is wind fed, the spin-up at a given mass accretion rate is always less than the spin-up rate in the disk-fed case, so that the magnetic moment calculated for the disk-fed case will be a lower limit for the wind-fed case. The expected spin-up rate for disk accretion is (see, e.g., Pringle & Rees 1972)

$$\dot{\nu} = (2\pi I)^{-1} \eta (GM r_A)^{1/2} \dot{M}, \quad (1)$$

where  $I$  is the neutron star’s moment of inertia,  $M$  its mass,  $\dot{M}$  the accretion rate onto the neutron star, and  $r_A$  the Alfvén radius for spherical accretion,

$$r_A = (2GM)^{-1/7} \mu^{4/7} \dot{M}^{-2/7}, \quad (2)$$

where  $\mu$  is the neutron star’s magnetic moment. The model-dependent factor  $\eta$  is expected to be near 1 in the “slow rotator” regime, where the rotation rate of the neutron star is much smaller than the rotation rate of the inner disk. For example, in the model of Ghosh & Lamb (1979, their eqs. [10] and [11]) this factor is given by  $\eta = n(0)\zeta^{1/2} (=1.39 \times 0.52^{1/2} = 1.00)$  for a slow rotator.

From the 94 s period change between MJD 52,717.84 and 52,724.39 seen in the *INTEGRAL* data, we infer an average spin-up rate of  $\dot{\nu} = 4.7 \times 10^{-12} \text{ Hz s}^{-1}$  ( $\dot{P} = 1.6 \times 10^{-4}$ ). For the same time interval we estimate an average unabsorbed 2–100 keV flux of  $F = 7 \times 10^{-10} \text{ ergs cm}^{-2} \text{ s}^{-1}$ , using flux estimates from the joint *INTEGRAL-Chandra* fit of  $1.2 \times 10^{-9} \text{ ergs cm}^{-2} \text{ s}^{-1}$  during Rev 52 and  $5.0 \times 10^{-10} \text{ ergs cm}^{-2} \text{ s}^{-1}$  at the time of the initial *Chandra* observation, combined with the trend of the IBIS/ISGRI 20–45 keV rates. With these values we find from equations (1) and (2) the magnetic moment

$$\mu = 1.8 \times 10^{32} \eta^{-7/2} m_{1.4}^{3/2} R_6^{-3} I_{45}^{7/2} d_7^{-6} \text{ G cm}^3, \quad (3)$$

where  $m_{1.4} = M/1.4 M_\odot$ ,  $R_6 = R/10^6 \text{ cm}$ ,  $I_{45} = I/10^{45} \text{ g cm}^2$ , and  $d_7 = d/7 \text{ kpc}$ . Figure 14 shows the magnetic moment (and field) as a function of distance to the source assuming canonical neutron star mass and radius.

As the mass accretion rate drops, the disk inner radius (or the magnetospheric radius)  $r_0 = \zeta r_A$  will expand to the corotation radius  $r_{\text{co}} = (GM)^{1/3} (2\pi/P)^{-2/3}$ , at which point the accretion will halt because material at  $r_0$  that is forced to corotate with the magnetic field is flung off by the centrifugal force (Illarionov & Sunyaev 1975). The transition to this “propeller regime” should occur when the accretion flux of IGR J16358–4726 decreases to

$$F_{\text{min}} = 1.6 \times 10^{-12} \eta^{-7} \zeta^{7/2} m_{1.4}^{7/3} R_6^{-7} I_{45}^7 d_7^{-14} \text{ ergs cm}^{-2} \text{ s}^{-1}. \quad (4)$$

IGR J16358–4726 was detected in the *XMM-Newton* observations with a 1–10 keV flux of  $7 \times 10^{-13} \text{ ergs cm}^{-2} \text{ s}^{-1}$ . The

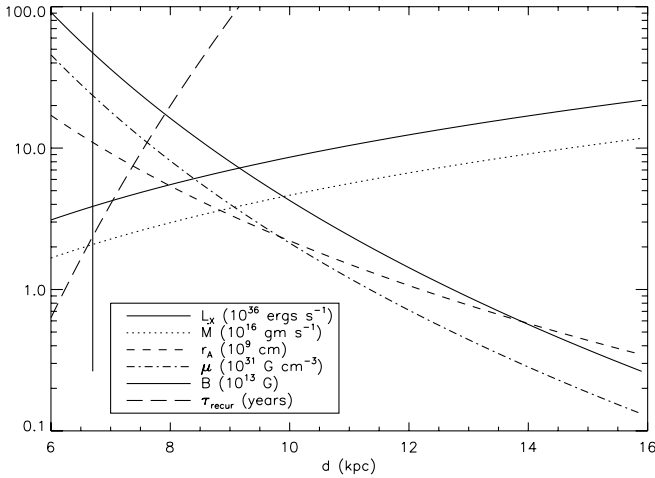


FIG. 14.—IGR J16358–4726 2–100 keV luminosity, mass accretion rate, Alfvén radius, magnetic moment, polar magnetic field strength, and recurrence time plotted as a function of distance. The y-axis units for each line are described in the legend. The lines assume canonical neutron star mass, radius, and moment of inertia of  $m_{1.4} = 1$ ,  $R_6 = 1$ , and  $I_{45} = 1$ , respectively. The vertical solid line reflects the lower limit on the distance based on our 2004 *XMM-Newton* measurement.

spectrum was hard and pulsations clearly present, both indicating that the neutron star was still accreting. This gives us a lower limit on the distance to the source of

$$d > 6.7(\epsilon/0.25)^{1/4} \eta^{-1/2} \zeta^{-1/4} m_{1.4}^{1/6} R_6^{-1/2} I_{45}^{1/2} \text{ kpc}, \quad (5)$$

where  $\epsilon$  is the fraction of the total flux in the 1–10 keV band.

The neutron star in IGR J16358–4726 was most likely born with a much shorter period than currently observed and has been spun down to its current state. Davies & Pringle (1981) discussed this spin evolution in the context of wind accreting systems and showed that obtaining long-period systems such as IGR J16358–

4726 requires a combination of high magnetic moment and low mass capture rates from the stellar wind. The impact of accretion disk formation on this evolution is unclear. If we suppose that the source is currently near an equilibrium period, with intervals of spin-up balanced by intervals of spin-down, then an interesting question is, how long are the spin-down intervals? If the source falls back into the subsonic propeller regime between outbursts, the spin-down rate will be (Davies & Pringle 1981)

$$\dot{P}_{\text{prop}} = 7 \times 10^{-4} \mu_{30}^2 m_{1.4}^{-1} I_{45}^{-1} \text{ s yr}^{-1}, \quad (6)$$

where  $\mu_{30} = \mu/10^{30} \text{ G cm}^3$ . So the time needed to recover the 94 s period decrease seen during the outburst is

$$\tau_{\text{recur}} = 94 \text{ s} / \dot{P}_{\text{prop}} = 3.5 \eta^7 m_{1.4}^{-2} R_6^6 I_{45}^{-6} d_7^{12} \text{ yr}, \quad (7)$$

so that if the distance to the source is greater than 8.4 kpc, we are not likely to see another outburst from it in the next 30 yr. The accretion disk solutions of Rappaport et al. (2004) show spin-down at low mass accretion rates that scale as equation (6), but with a factor of 6 lower rate. If, in fact, the recurrence time is this long, we consider the fact that the transient was detected in outburst for the first time during the initial year of *INTEGRAL* Galactic plane scans as extremely fortuitous. Therefore, if the source is detected in a similar state again within the next 3.5 yr, it most likely is a transiently accreting magnetar at  $\sim 7$  kpc with a field strength of  $3.4 \times 10^{14} \text{ G}$ .

S. K. P. acknowledges support from NASA grants NNG04GH33G and DD3-4023X. M. D. S. has been supported by the Italian Space Agency grant I/R/046/04. D. E. acknowledges the Israel Science Foundation, the US-Israel Binational Science Foundation, and the Arnow Chair of Theoretical Astrophysics. We thank E. Behar for discussions on the nature of the spectral lines.

#### REFERENCES

- Alpar, M. A. 1977, *ApJ*, 213, 527  
 Anderson, P. W., & Itoh, N. 1975, *Nature*, 256, 25  
 Arnaud, K. A. 1996, in *ASP Conf. Ser. 101, Astronomical Data Analysis Software and Systems V*, ed. G. H. Jacoby & J. Barnes (San Francisco: ASP), 17  
 Bildsten, L., et al. 1997, *ApJS*, 113, 367  
 Buccheri, R., et al. 1983, *A&A*, 128, 245  
 Cash, W. 1979, *ApJ*, 228, 939  
 Churazov, E., Gilfanov, M., Forman, W., & Jones, C. 1996, *ApJ*, 471, 673  
 Corbet, R., et al. 2005, *Astron. Tel.*, 649, 1  
 Courvoisier, T. J.-L., et al. 2003, *A&A*, 411, L53  
 D’Amico, F., Jablonski, F., Rodrigues, C. V., Cieslinski, D., & Hickel, G. 2006, in *AIP Conf. Proc. 840, The Transient Milky Way: A Perspective for MIRAX*, ed. F. D’Amico, J. Braga, & R. E. Rothschild (New York: AIP), 97  
 Davies, R. E., & Pringle, J. E. 1981, *MNRAS*, 196, 209  
 Galloway, D. K., Morgan, E. H., & Levine, A. M. 2004, *ApJ*, 613, 1164  
 Ghosh, P., & Lamb, F. K. 1979, *ApJ*, 234, 296  
 Gros, A., Goldwurm, A., Cadolle-Bel, M., Goldoni, P., Rodriguez, J., Foschini, L., Del Santo, M., & Blay, P. 2003, *A&A*, 411, L179  
 Heyl, J. S., & Hernquist, L. 1999, *MNRAS*, 304, L37  
 Illarionov, A. F., & Sunyaev, R. A. 1975, *A&A*, 39, 185  
 Kaspi, V. M., Gavriil, F. P., Woods, P. M., Jensen, J. B., Roberts, M. S. E., & Chakrabarty, D. 2003, *ApJ*, 588, L93  
 Kaspi, V. M., Lackey, J. R., & Chakrabarty, D. 2000, *ApJ*, 537, L31  
 Kouveliotou, C., Patel, S., Tennant, A., Woods, P., Finger, M., & Wachter, S. 2003a, *IAU Circ.*, 8109, 2  
 Kouveliotou, C., et al. 2003b, *ApJ*, 596, L79  
 Krawczyk, A., Lyne, A. G., Gil, J. A., & Joshi, B. C. 2003, *MNRAS*, 340, 1087  
 Kuulkers, E. 2005, in *AIP Conf. Proc. 797, Interacting Binaries: Accretion, Evolution, and Outcomes*, ed. L. Burderi et al. (New York: AIP), 402  
 Lebrun, F., et al. 2003, *A&A*, 411, L141  
 Lutovinov, A., Revnivtsev, M., Gilfanov, M., Shtykovskiy, P., Molkov, S., & Sunyaev, R. 2005, *A&A*, 444, 821  
 Morii, M., Kawai, N., & Shibazaki, N. 2005, *ApJ*, 622, 544  
 Pandey, M., Manchanda, R. K., Rao, A. P., Durouchoux, P., & Ishwara-Chandra, C. H. 2006, *A&A*, 446, 471  
 Patel, S. K., et al. 2004, *ApJ*, 602, L45  
 Pringle, J. E., & Rees, M. J. 1972, *A&A*, 21, 1  
 Rappaport, S. A., Fregeau, J. M., & Spruit, H. 2004, *ApJ*, 606, 436  
 Revnivtsev, M., Tuerler, M., Del Santo, M., Westergaard, N. J., Gehrels, N., & Winkler, C. 2003, *IAU Circ.*, 8097, 2  
 Revnivtsev, M. G. 2003, *Astron. Lett.*, 29, 644  
 Ruderman, M. 1976, *ApJ*, 203, 213  
 Scargle, J. D. 1982, *ApJ*, 263, 835  
 Shemar, S. L., & Lyne, A. G. 1996, *MNRAS*, 282, 677  
 Titarchuk, L. 1994, *ApJ*, 434, 570  
 Ubertini, P., et al. 2003, *A&A*, 411, L131  
 Wilms, J., Allen, A., & McCray, R. 2000, *ApJ*, 542, 914  
 Winkler, C., et al. 2003, *A&A*, 411, L1  
 Yan, M., Sadeghpour, H. R., & Dalgarno, A. 1998, *ApJ*, 496, 1044